Frequency-Dependent Impedance Matching Synthesis Methodology for Filters or Matching Networks With Equiripple Responses

Santi Cano, *Graduate Student Member, IEEE*, Mario Faura, *Graduate Student Member, IEEE*, Laia Garcia, *Graduate Student Member, IEEE*, Josep Parrón-Granados, *Senior Member, IEEE*, and Pedro de Paco, *Senior Member, IEEE*

***Abstract*—Current synthesis techniques rely on either the lowpass prototype (LP) or direct bandpass (DB) representations to analyze filtering responses, each offering its own advantages. However, all these synthesis methods are carried out under the assumption that both the source and load terminations are constant impedances. This assumption is unrealistic for most RF filter designs, as they are often required to be matched to real devices with frequency-dependent impedances [$Z_L(f)$]. The problem can be interpreted as the interaction between two networks: S_A, representing the filter, and S_B, representing the $Z_L(f)$. When cascaded, these networks produce an overall response S_T. This article presents a direct synthesis approach for designing general Chebyshev filters terminated with a $Z_L(f)$ at one port. The proposed approach employs a Remez-like algorithm to determine the characteristic polynomials of S_A such that, when cascaded with S_B, the overall response S_T exhibits an in-band quasi-equiripple behavior. Moreover, the proposed approach provides flexibility in controlling the return loss level (RL_T) of S_T, which is particularly useful for adjusting the out-of-band (OoB) rejection level and accommodating technological constraints in certain RF filters. The proposed method is validated through two examples with different optimality criteria: 1) an all-pole filter matched to an antenna booster, designed to approach the Bode–Fano limit by including the antenna's reflection zero (RZ) within the quasi-equiripple response of S_T, thereby achieving the most optimal solution; and 2) a ladder filter matched to a real switch, designed excluding its RZs from S_T to obtain a suboptimal solution.**

***Index Terms*—Acoustic wave (AW) ladder filters, Bode–Fano limit, cascaded filter, Chebyshev polynomials, equiripple behavior, frequency-dependent load impedance, matching network.**

I. Introduction

In RECENT decades, the demand for radio frequency (RF) filters in mobile devices has grown significantly [1], [2], [3], [4]. Consequently, the research community has extensively demonstrated that synthesis techniques enable a much faster exploration of different filtering functions and topologies compared to traditional optimization processes, thereby assisting designers in identifying the most suitable filter for a given technology and set of specifications.

The synthesis of filters is commonly carried out using lowpass prototype (LP) techniques, which offer an excellent tradeoff between effectiveness and simplicity for addressing narrowband filter designs [5], [6], [7]. These methods employ reduced-order filtering polynomials and enable asymmetric responses by introducing frequency-invariant reactance (FIR) elements. However, they inherently neglect the behavior at extreme frequencies, limiting their applicability in wideband scenarios. Another alternative is the direct bandpass (DB) synthesis techniques [8], [9], [10], which allow modeling the behavior of the filter across the entire frequency spectrum, but are more complex and require polynomials with twice the order of those used in LP approaches. Both LP and DB techniques involve a sequence of analytical steps that do not require any optimization. First, a set of characteristic polynomials is derived based on the prescribed specifications, typically defining a generalized Chebyshev filtering function with equiripple behavior in the passband to ensure optimal out-of-band (OoB) rejection [11]. Then, through a fully deterministic procedure, these polynomials are translated into the circuit elements that implement the desired filtering function in the filter. This translation can be carried out using the extracted-pole technique, typically applied in the LP case as described in [5] and [12] and extended to the DB case in [8], or alternatively using the coupling matrix approach [11], [13], also applied in the LP and extended to the DB in [9].

However, a fundamental limitation of current LP and DB techniques lies in the assumption that the filter is matched to a constant load impedance (Z_L). This assumption is valid only when the filter operates over a very narrow fractional bandwidth (FBW) and the actual frequency-dependent load impedance [$Z_L(f)$] exhibits minimal dispersion around this assumed constant Z_L. Otherwise, when cascading the synthesized filter with the $Z_L(f)$, the expected

Received 9 January 2026; revised 23 February 2026; accepted 12 March 2026. This work was supported in part by the Agencia Estatal de Investigacion (AEI)–Ministerio de Ciencia e Innovación under Project PID2024-159605OB-I00 and in part by the Departament d'Universitats i Recerca. *(Corresponding author: Santi Cano.)*

The authors are with the Department of Telecommunications and Systems Engineering, Universitat Autónoma de Barcelona, 08193 Bellaterra, Spain (e-mail: santi.cano@uab.cat).

Digital Object Identifier 10.1109/TMTT.2026.3674572

response deteriorates significantly, sometimes even preventing compliance with specifications. Matching the filter directly to a $Z_L(f)$ is a critical step in the successful design of RF front-end modules, where different components, such as antennas, switches, power amplifiers, low-noise amplifiers, and other RF front-end elements must be interconnected with stand-alone filters, notch filters, duplexers, or multiplexers [4].

Research efforts have been dedicated to the synthesis of filters matched to complex $Z_L(f)$. The matching problem dates back to the foundational work of Fano [14], who developed a synthesis procedure for matching networks based on the derivation of a lossless two-port scattering matrix representing the filter connected to the antenna. However, it does not guarantee an equiripple optimal solution and relies on nonconvex optimizations, which result in multiple local minima that do not guarantee a closed-form solution. Carlin and Civalleri [15] introduced a nonconvex optimization method that works directly with real frequency functions, aiming to synthesize a matching network based on a given reflection or scattering function. Nevertheless, equiripple solutions cannot be obtained, and the global optimality of the solution is not guaranteed. Helton [16] reformulated the problem as a quasi-convex optimization minimizing the pseudohyperbolic distance, which allows achieving a globally optimal response at the cost of requiring an infinite-dimensional matching network, something that cannot be physically realized. More recently, Martinez [17] and Bose et al. [18] proposed a practical way to apply Helton's method using Nehari's theory to convert nonrealizable functions into realizable approximations in H^∞, allowing the computation of the best possible approximation for a realizable filter.

These prior works rely on pure optimization methods rather than finding a numerical solution to the problem. To the best of the author's knowledge, a numerical approach for synthesizing filters matched to a $Z_L(f)$ has not yet been addressed within the filter design community. This work introduces a novel numerical method for synthesizing filters with quasi-equiripple behavior in the presence of a $Z_L(f)$, as long as it can be represented as a rational function. Throughout this work, the $Z_L(f)$ of all examples is modeled using the vector fitting technique proposed by Bose et al. [19], Gustavsen and Semlyen [20], Gustavsen [21], and Deschrijver et al. [22], which fits measured or simulated frequency-domain responses with rational function approximations. Instead of using the LP approximation of [5] to synthesize the RF filters, this work utilizes the DB approach proposed in [8], because the fit Touchstone files that contain the information of the actual $Z_L(f)$ are always defined in the DB domain. Due to the author's interest, the method is derived, without loss of generality, for ladder networks under the acoustic wave (AW) technological constraints imposed by piezoelectric resonators. Nevertheless, the proposed methodology remains applicable to any other filter technology or topology, since it is based on the polynomial formulation of the filtering function.

Fig. 1 depicts the cascade of two lossless two-port networks, S_A and S_B, whose cascade results in the total network

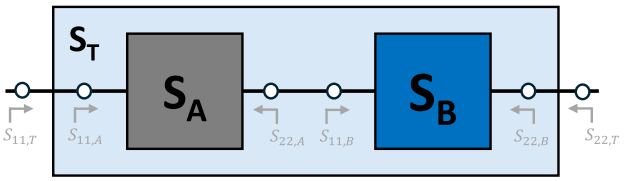

Fig. 1. Block diagram illustrating the cascaded S parameters of two lossless two-port networks, S_A and S_B, resulting in the total network S_T.

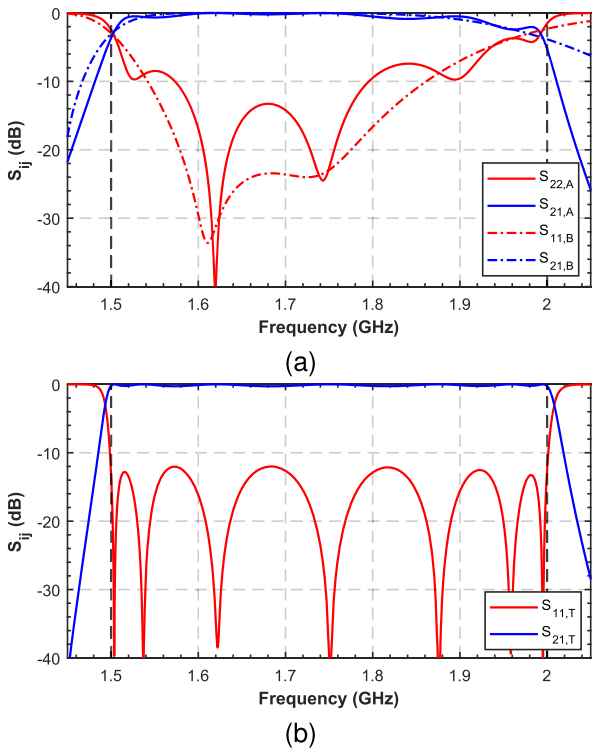

Fig. 2. Cascading between a synthesized fifth-order ladder filter S_A and a second-order S_B. (a) Individual responses of S_A and S_B, both matched to a constant $Z_S = Z_L = 50\ \Omega$. (b) Response of the cascaded network S_T.

S_T. Throughout this work, S_A denotes the filter, S_B models the $Z_L(f)$ network, and S_T corresponds to their whole and cascaded response, all referenced to 50-Ω source and load impedances. The proposed methodology avoids computationally intensive optimization procedures by leveraging a Remez-like algorithm to compute the distorted polynomials of S_A such that, once cascaded with those of S_B, the resulting S_T exhibits a quasi-equiripple response. Fig. 2(a) illustrates this behavior cascading a fifth order ladder filter network $S_{11,A}$ with a second order $S_{11,B}$. When setting a total return loss (RL_T) level of 12 dB, the reflection coefficient $S_{11,A}$ is distorted when referenced to a $Z_L = 50\ \Omega$. However, when cascaded with $S_{11,B}$, the resulting $S_{11,T}$ shown in Fig. 2(b) exhibits a quasi-equiripple response at the desired RL_T level. This behavior is observed from an impedance perspective in Fig. 3(a) and (b), where both the real and imaginary parts of $Z_{out,A}(f)$ oscillate around the complex conjugate dispersive impedance $Z^*_{in,B}(f)$ to obtain the desired equiripple level. In addition, this methodology offers the advantage of flexibility in selecting the RL_T level, which is particularly useful

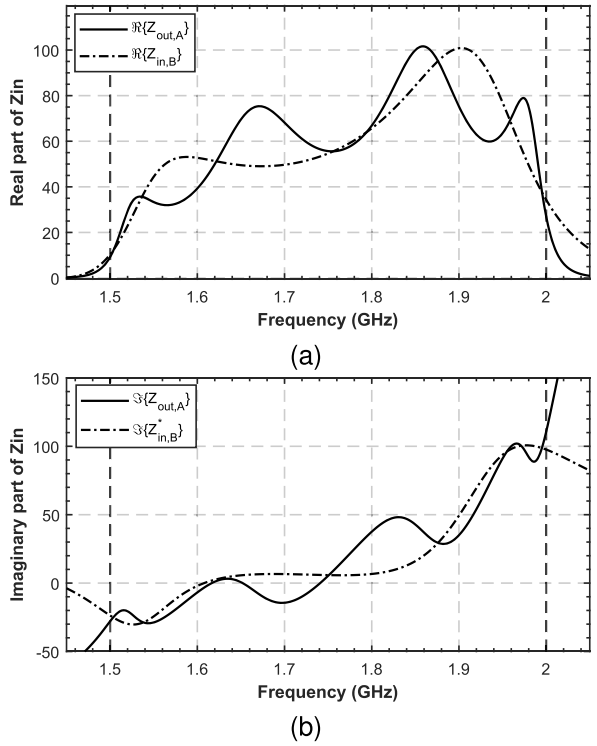

Fig. 3. Output $Z_{out,A}$ and input $Z^*_{in,B}$ impedances of S_A and S_B, respectively. (a) Real parts. (b) Imaginary parts.

for controlling the OoB rejection and for accommodating technological constraints, such as the electromechanical coupling coefficient k_t^2 in AW technology [5], [23].

This work proposes two different approaches in terms of optimality when matching the filter to a $Z_L(f)$. The first approach corresponds to the optimal solution [17] and consists of including the reflection zeros (RZs) of $Z_L(f)$ in S_T, as illustrated in Fig. 2. This approach allows S_T to behave as a higher-order filter, since it accounts not only for the RZs of S_A but also for those of S_B. As a result, the RL_T and the OoB rejection are the best. Certainly, this represents the best possible solution. However, there are situations in which $Z_L(f)$ is too complex to be accurately modeled, or its RZs cannot appear in the quasi-equiripple response of S_T because they lie outside the passband. For this reason, the second approach consists of matching the filter to $Z_L(f)$ while excluding its RZs. In this case, S_T behaves as a filter of the same order as S_A. Consequently, the achievable RL_T is reduced, and the OoB rejection is worse because the RZ of S_B are located somewhere in the complex plane outside the passband of S_T. To evaluate the effectiveness of the two proposed approaches for different filter topologies and technologies, two representative examples are presented. In the first case, a third-order all-pole filter matched to an antenna booster is designed to approach the Bode–Fano limit by including the antenna RZ in the overall response S_T. The second example considers a fifth-order AW ladder filter matched to a real switch, synthesized by excluding the RZs of S_B from S_T. This results in a suboptimal response that nevertheless preserves an in-band quasi-equiripple behavior by relying exclusively on the RZs of S_A.

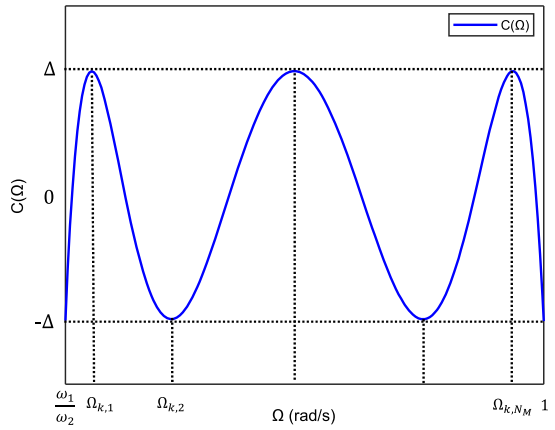

Fig. 4. Characteristic function $C(\Omega)$ of the positive frequency passband of a N_Mth-order Chebyshev filter in the DB domain.

II. Synthesis of Filters Considering Constant Z_L in the DB Domain

For completeness, this section first introduces the Remez-like algorithm used to generate the ideal DB Chebyshev function for ladder filters matched to constant source and load impedances. Let us start by defining the S parameters by means of the characteristic polynomials $P(s)$, $F(s)$, and $E(s)$ of a filter function [11, ch. 6] in the normalized domain $s = \Sigma + j\Omega$

$$\begin{bmatrix} S_{11}(s) & S_{12}(s) \\ S_{21}(s) & S_{22}(s) \end{bmatrix} = \frac{1}{E(s)} \begin{bmatrix} F(s) & P(s)/\varepsilon \\ P(s)/\varepsilon & (-1)^N F(s)^* \end{bmatrix} \quad (1)$$

where ε is the normalization constant that ensures $P(s)$ is a monic polynomial, and the roots of $P(s)$, $F(s)$, and $E(s)$ correspond to the transmission zeros (Ω_{TZ}), RZs, and poles of the ladder topology, respectively. As detailed in [8], the DB approach oriented to ladder filters requires the use of a not-fully canonical filtering function, where the computed characteristic polynomials form a dual-band response symmetric about zero, and that can be asymmetric with respect to the center frequency. Accordingly, the negative and positive frequency passbands span $\Omega \in \{-1, -\omega_1/\omega_2\}$ and $\Omega \in \{\omega_1/\omega_2, 1\}$, respectively. To construct the proposed filtering function, the Remez-like algorithm requires defining a filter order of $N_{DB} = 2N + 2$. For a ladder topology, polynomial $P(s)$ contains N positive Ω_{TZ} and their N negative symmetric counterparts, one Ω_{TZ} at the origin and one at infinity. In contrast, polynomial $F(s)$ contains N positive RZs and their N negative symmetric counterparts, which shape the two equiripple passbands, as well as a pair of imaginary RZs ($j\Omega_{RZ}$) that model the frequency-dependent input and output phase behavior. Note that the prescribed Ω_{TZ} and $j\Omega_{RZ}$ have been defined for a ladder network with input and output capacitors, but the definition of the filtering function may be different depending on the network.

A. Interpretation of the Remez Algorithm in the DB Domain

According to the formulation in [24], the polynomial $F(\Omega)$ is defined such that $N_M = N_{DB} - N_{j\Omega_{RZ}}$ represents the total in-band order, $N_1 = N_2 = N_M/2$ represents the order of each

passband, and $N_{j\Omega_{RZ}}$ represents the number of prescribed $j\Omega_{RZ}$ that accommodate the frequency-dependent input and output phases. The FBW of both passbands is determined by the desired cut-off frequencies, with $\Omega = \pm 1$ being the furthest from zero and $\Omega = \pm\omega_1/\omega_2$ being the closest to zero for both passbands. Let F_0 be the monic polynomial whose roots define the RZs of each passband. Its N_M unknown coefficients $\{f_k\}$ describe the equiripple characteristic function $C(\Omega)$ in each passband, which, as illustrated in Fig. 4, oscillates with constant amplitude $\pm\Delta$ and can be expressed as

$$C(\Omega) = |F_C(j\Omega)| \cdot F_0(\Omega)/P(\Omega) \tag{2}$$

where $F_C(j\Omega)$ is the monic polynomial of degree $N_{j\Omega_{RZ}}$ containing the assigned $j\Omega_{RZ}$.

The monic polynomial $F_0(\Omega)$ is commonly found by iteratively solving a linear system at the extrema points $\Omega_{k,i}$, where $|\Delta_k|$ becomes maximum or minimum

$$C(\Omega_{k,i}) = \frac{|F_C(j\Omega_{k,i})| \cdot F_0(\Omega_{k,i})}{P(\Omega_{k,i})} = (-1)^{i-1}|\Delta_k| \tag{3}$$

where $k = 1, 2$ and $i = 1, 2, \ldots, N_M + 2$. Expressing $F_0(\Omega_{k,i})$ in terms of its coefficients $\{f_1, f_2, \ldots, f_{N_M}\}$, (3) can be reformulated as

$$f_2\Omega_{k,i}^{N_M-1} + \cdots + f_{N_M} - \frac{(-1)^{i-1}|\Delta_k| P(\Omega_{k,i})}{|F_C(\Omega_{k,i})|} = -f_1\Omega_{k,i}^{N_M} \tag{4}$$

where $f_1 = 1$ is the coefficient of the highest-degree term, and f_{N_M} is the constant term associated with degree zero.

Then, the iterative process is described in five steps.

1) *Step 1:* Initialize the $N_M + 2$ symmetric frequency sample points $\Omega_{k,i} = \{\Omega_{1,i}\} \cup \{\Omega_{2,i}\}$, evenly distributed in each passband.
2) *Step 2:* Solve the $N_M + 2$ linear system of equations at $\Omega_{k,i}$ to obtain the N_M unknown coefficients of $F_0(\Omega)$ and the two equal amplitudes Δ_k of both in-band ripples of $C(\Omega)$. Therefore, the linear system is stated by isolating $F_0(\Omega_{k,i})$ from $|F_C(j\Omega_{k,i})| \cdot F_0(\Omega_{k,i})/P(\Omega_{k,i}) = (-1)^{i-1}\Delta_k$ as
$$\boldsymbol{A} \cdot \boldsymbol{x} = \boldsymbol{v}. \tag{5}$$
Equation (5) can also be written as in (6), shown at the bottom of the page.
3) *Step 3:* Update the frequency sample points Ω_i' computing the zeros of the derivative of $C(\Omega)$
$$\frac{\partial C(\Omega)}{\partial \Omega} = 0. \tag{7}$$
The in-band roots of each passband and their respective band limits $[-1, -\omega_1/\omega_2]$ and $[\omega_1/\omega_2, 1]$ rad/s will be the $N_M + 2$ updated frequency sample points Ω_i' once the OoB turning points are removed.
4) *Step 4:* Repeat steps 2 and 3 until convergence considering $max|\Omega_i - \Omega_i'|$ is small enough (e.g., less than 10^{-5}).
5) *Step 5:* After the iterations, $F(s)$ and $P(s)$ can be derived from $F(\Omega)$ and $P(\Omega)$ using $s = j\Omega$ and $E(s)$ can be obtained using the Feldtkeller's equation [11]
$$E(s)E^*(s) = F(s)F^*(s) + \frac{P(s)P^*(s)}{\varepsilon^2} \tag{8}$$
where the notation "*" denotes the paraconjugate of the polynomial.

III. Synthesis of Filters Considering Frequency-Dependent $Z_L(f)$ in the DB Domain

In the iterative polynomial synthesis procedure with constant Z_L introduced in Section II, the roots of $F_{0,A}(\Omega)$ are constrained to lie on the real axis of Ω, and the equiripple condition is strictly enforced.

However, when the Z_L becomes $Z_L(f)$, the filter network S_A will no longer exhibit an equiripple response, as the goal now is to achieve this behavior in S_T. As illustrated in Fig. 5, the in-band RZs of S_A must move off the real axis into the complex plane to preserve a quasi-equiripple match in S_T once S_B is cascaded.

Before delving into the extended Remez-like algorithm to account for the $Z_L(f)$, it is necessary to first define how the S parameters of two passive reciprocal cascaded networks, S_A and S_B, interact with each other. To begin with, the transmission parameter of the total response $S_{21,T}$ is defined in terms of the characteristic polynomials of each network as

$$S_{21,T}(\Omega) = \frac{S_{21,A}(\Omega)S_{21,B}(\Omega)}{1 - S_{22,A}(\Omega)S_{11,B}(\Omega)} \tag{9}$$

$$\frac{P_T(\Omega)}{\varepsilon_T E_T(\Omega)} = \frac{P_A(\Omega)P_B(\Omega)}{\varepsilon_A\varepsilon_B\left[E_A(\Omega)E_B(\Omega) - \dfrac{F_A^*(\Omega)F_B(\Omega)}{\varepsilon_{r,A}\varepsilon_{r,B}}\right]} \tag{10}$$

$$\begin{bmatrix}
\Omega_{1,1}^{N_M-1} & \Omega_{1,1}^{N_M-2} & \cdots & 1 & \frac{(-1)^1 P(\Omega_{1,1})}{|F_C(\Omega_{1,1})|} & 0 \\
\Omega_{1,2}^{N_M-1} & \Omega_{1,2}^{N_M-2} & \cdots & 1 & \frac{(-1)^2 P(\Omega_{1,2})}{|F_C(\Omega_{1,2})|} & 0 \\
\vdots & \vdots & \vdots & \vdots & \vdots & \vdots \\
\Omega_{1,N_1+1}^{N_M-1} & \Omega_{1,N_1+1}^{N_M-2} & \cdots & 1 & \frac{(-1)^{N_1+1} P(\Omega_{1,N_1+1})}{|F_C(\Omega_{1,N_1+1})|} & 0 \\
\Omega_{2,1}^{N_M-1} & \Omega_{2,1}^{N_M-2} & \cdots & 1 & 0 & \frac{(-1)^1 P(\Omega_{2,1})}{|F_C(\Omega_{2,1})|} \\
\Omega_{2,2}^{N_M-1} & \Omega_{2,2}^{N_M-2} & \cdots & 1 & 0 & \frac{(-1)^2 P(\Omega_{2,2})}{|F_C(\Omega_{2,2})|} \\
\vdots & \vdots & \vdots & \vdots & \vdots & \vdots \\
\Omega_{2,N_2+1}^{N_M-1} & \Omega_{2,N_2+1}^{N_M-2} & \cdots & 1 & 0 & \frac{(-1)^{N_2+1} P(\Omega_{2,N_2+1})}{|F_C(\Omega_{2,N_2+1})|}
\end{bmatrix}
\begin{bmatrix} f_2 \\ f_3 \\ \vdots \\ f_{N_M} \\ \Delta_1 \\ \Delta_2 \end{bmatrix}
=
\begin{bmatrix}
-\Omega_{1,1}^{N_M} \\ -\Omega_{1,2}^{N_M} \\ \vdots \\ -\Omega_{1,N_1+1}^{N_M} \\ -\Omega_{2,1}^{N_M} \\ -\Omega_{2,2}^{N_M} \\ \vdots \\ -\Omega_{2,N_2+1}^{N_M}
\end{bmatrix} \tag{6}$$

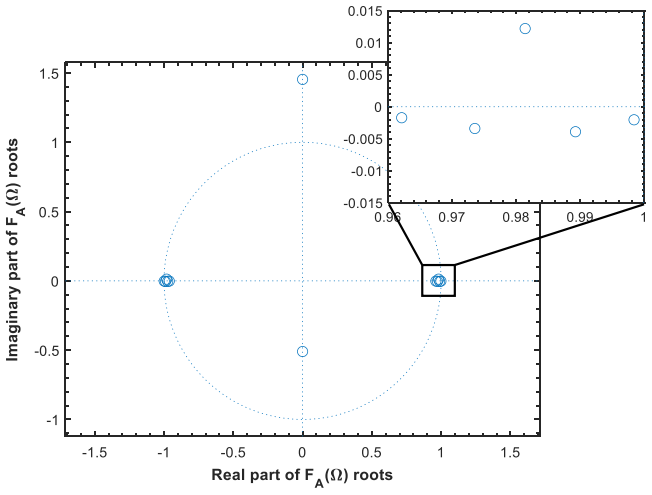

Fig. 5. Roots diagram of $F_A(\Omega)$.

whereas the input reflection parameter $S_{11,T}$ is defined as

$$S_{11,T}(\Omega) = S_{11,A}(\Omega) + \frac{S_{21,A}^2(\Omega) S_{11,B}(\Omega)}{1 - S_{22,A}(\Omega) S_{11,B}(\Omega)} \tag{11}$$

$$\frac{F_T(\Omega)}{E_T(\Omega)} = \frac{F_A(\Omega) E_B(\Omega) - \dfrac{\varepsilon_{r,A} F_B(\Omega) E_A^*(\Omega)}{\varepsilon_{r,B}}}{E_A(\Omega) E_B(\Omega) - \dfrac{F_A^*(\Omega) F_B(\Omega)}{\varepsilon_{r,A}\varepsilon_{r,B}}} \tag{12}$$

and the output reflection parameter $S_{22,T}$ as

$$S_{22,T}(\Omega) = S_{22,B}(\Omega) + \frac{S_{21,B}^2(\Omega) S_{22,A}(\Omega)}{1 - S_{22,A}(\Omega) S_{11,B}(\Omega)} \tag{13}$$

$$\frac{F_T^*(\Omega)}{E_T(\Omega)} = \frac{F_B^*(\Omega) E_A(\Omega) - \dfrac{\varepsilon_{r,A} F_A^*(\Omega) E_B^*(\Omega)}{\varepsilon_{r,B}}}{E_A(\Omega) E_B(\Omega) - \dfrac{F_A^*(\Omega) F_B(\Omega)}{\varepsilon_{r,A}\varepsilon_{r,B}}}. \tag{14}$$

Notice in (12) and (14) that since both networks must satisfy the Feldtkeller equation, the order of the resulting cascaded network, $N_{DB,T}$, is not $N_{DB,A} + N_{DB,B}$, but rather $N_{DB,A} + N_{DB,B} - 2$. This reduction by two occurs because: 1) the numerators and denominators in (12) and (14) involve subtractions between monic polynomials, which cancel the highest-order terms; and 2) their independent coefficients are also identical, resulting in a common root at $s = 0$ after subtraction that cancels out during division.

A. Remez-Like Algorithm Including the RZs of S_B in S_T

Knowing the relationship between the cascaded network S_T and the characteristic polynomials of the individual networks S_A and S_B, the Remez-like algorithm presented in Section II can be reformulated accordingly. The objective is to determine the $N_{M,A}$ unknown coefficients of $F_{0,A}(\Omega)$, which represent the N_A in-band complex RZs of S_A required to achieve a quasi-equiripple when considering S_B. Consequently, the characteristic function of the cascaded response $C_T(\Omega)$ must oscillate with a constant amplitude $\pm\Delta_T$, and thus (3) can be rewritten taking into account the characteristic polynomials of S_A and S_B as

$$C_T(\Omega) = \frac{F_{0,A}(\Omega) F_{C,A}(\Omega) E_B(\Omega) - \dfrac{\varepsilon_{r,A} F_B(\Omega) E_A^*(\Omega)}{\varepsilon_{r,B}}}{P_A(\Omega) P_B(\Omega)} \tag{15}$$

where $F_{C,A}(j\Omega)$ contains the assigned $j\Omega_{RZ,A}$ of S_A.

Expressing $F_{0,A}(\Omega)$ in terms of its coefficients, (15) can be reformulated as

$$f_{2,A}\Omega_{k,i}^{N_{M,A}-1} + \ldots + f_{N_{M,A}} - \frac{(-1)^{i-1}|\Delta_{k,T}|P_A(\Omega_{k,i})P_B(\Omega_{k,i})}{F_{C,A}(\Omega_{k,i})E_B(\Omega_{k,i})} = -\Omega_{k,i}^{N_{M,A}} + (-1)^{N_{M,A}} \frac{\varepsilon_{r,A} F_B(\Omega_{k,i}) E_A^*(\Omega_{k,i})}{\varepsilon_{r,B} F_{C,A}(\Omega_{k,i}) E_B(\Omega_{k,i})} \tag{16}$$

where $k = [1, 2]$ and $i = [1, 2, \ldots, N_{M,T} + 2]$. Let us highlight that (16) accounts only for the $N_{M,A} + 2$ extrema points associated with $F_{0,A}(\Omega_{k,i})$. However, to achieve the quasi-equiripple behavior with all the RZs, the contribution of $F_{0,B}(\Omega_{k,i})$ must also be considered. This requires a total in-band order of $N_{M,T} = N_{M,A} + N_{M,B}$ (or $N_{1,T} = N_{2,T} = N_{M,T}/2$ for each passband), and consequently, $N_{M,T} + 2$ extrema points should be contemplated when solving for $F_{0,A}(\Omega_{k,i})$, leading to an overdetermined system of equations.

Then, the iterative process is described in six steps.

1) *Step 1:* Compute $F_A(s)$ and $E_A(s)$ as explained in Section II. These conventional polynomials will be used as a starting point for the iterative procedure.
2) *Step 2:* Initialize the $N_{M,T} + 2$ symmetric frequency sample points $\Omega_{k,i} = \{\Omega_{1,i}\} \cup \{\Omega_{2,i}\}$, evenly distributed in each passband.
3) *Step 3:* Solve the $N_{M,A} + 2$ linear system of equations at $\Omega_{k,i}$ to determine the $N_{M,T}$ unknown coefficients of $F_{0,A}(\Omega_{k,i})$, along with the two equal amplitudes Δ_k that define in-band ripples of $C_T(\Omega_{k,i})$ at the upper band edges. The linear equations can be written in matrix form, similar to (5), as
$$\boldsymbol{A'} \cdot \boldsymbol{x} = \boldsymbol{v'}. \tag{17}$$
Equation (17) can also be written as in (18), shown at the bottom of the next page. Different from (5), (17) and (18) are overdetermined equations, and an exact solution does not exist. Nevertheless, an optimal approximate solution can be obtained through the least squares criteria, yielding a quasi-equiripple behavior when cascading S_A with S_B. The accuracy of this approximation depends on the order of S_B, with the solution becoming less precise as more RZs from S_B are taken into account.
4) *Step 4:* Having obtained $F'_A(\Omega) = F'_{0,A}(\Omega)F_{C,A}(\Omega)$ from (17), and using the $E_A(\Omega)$ from the previous iteration, provisional polynomials $P_T(\Omega)$ and $F_T(\Omega)$ can be computed using (10) and (12). These are used to evaluate the amplitude $|\Delta|$ at the extrema points Ω_i to identify the one that results in a $S_{11,T}$ lower than the required RL_T level, as follows:
$$\Omega_{i\max} = \arg\max_{\Omega_i} \left(\frac{|F_T(\Omega)|}{|P_T(\Omega)|} \right) \Bigg|_{\Omega=\Omega_i}. \tag{19}$$
This $\Omega_{i\max}$ allows the calculation of the normalization constant ε'_T that achieves the minimum RL_T, ensuring

that the resulting quasi-equiripple behavior satisfies the specified RL_T level throughout the entire passband

$$\varepsilon'_T = \frac{1}{\sqrt{10^{RL_T/10}-1}} \left| \frac{P_T(\Omega)}{F_T(\Omega)} \right|_{\Omega=\Omega_{i\max}}. \tag{20}$$

Then, the new polynomial $E'_A(s)$ can be computed through the Feldtkeller equation as

$$E'_A(s)\,E'^*_A(s) = F'_A(s)\,F'^*_A(s) + \frac{P_A(s)\,P^*_A(s)}{\varepsilon'^2_A} \tag{21}$$

where $s = j\Omega$ and

$$\varepsilon'_A = \varepsilon'_T/\varepsilon_B. \tag{22}$$

5) *Step 5:* From (10) and (12), compute the updated characteristic polynomials of the cascaded response $P_T(s)$, $F'_T(s)$, and $E'_T(s)$, this time considering the updated $E'_A(s)$ of (21). Since the zeros of $F'_T(s)$ may lie in the complex plane, the updated extrema points Ω'_i can no longer be directly obtained by differentiating the characteristic function, as in (7). Instead, all new extrema points Ω'_i must be determined by differentiating the power characteristic within the passband [11]

$$\frac{\partial\left(S_{21}(s)S^*_{21}(s)\right)}{\partial s} = \frac{\partial\left[\frac{P_T(s)P^*_T(s)}{P_T(s)P^*_T(s)+F'_T(s)F'^*_T(s)}\right]}{\partial s} = 0. \tag{23}$$

By expanding the numerator polynomial of (23), the solutions are obtained as follows:

$$\left[\left(\frac{\partial P_T(s)}{\partial s}P^*_T(s) + P_T(s)\frac{\partial P^*_T(s)}{\partial s}\right)F'_T(s)\,F'^*_T(s) - P_T(s)\,P^*_T(s)\left(\frac{\partial F'_T(s)}{\partial s}F'^*_T(s) + F'_T(s)\frac{\partial F'^*_T(s)}{\partial s}\right)\right] = 0. \tag{24}$$

The roots of (24) represent both in-band and OoB turning points, including off-axis RZs. Since some RZs may fall outside the passband, the updated extrema points $\Omega'_i = -js'_i$ must be selected alternately from the $2\cdot(N_{M,T}-1)$ closest in-band solutions, while also including the band edges at $[\pm\omega_1/\omega_2, \pm 1]$ rad/s.

6) *Step 6:* Repeat steps 3–5 until convergence considering $max|\Omega_i - \Omega'_i|$ is small enough (e.g., less than 10^{-4}).

After convergence of the iterative procedure, the resulting characteristic polynomials P_A, F'_A, and E'_A define a distorted filter response S_A similar to that of Fig. 2(a). When cascading this S_A response with the $Z_L(f)$ associated with S_B, the resulting response S_T will exhibit a quasi-equiripple behavior that meets the prescribed RL_T level, as in Fig. 2(b).

B. Remez-Like Algorithm Excluding the RZs of S_B From S_T

The computation of the characteristic polynomials of S_A that produce a suboptimal quasi-equiripple response

$$\begin{bmatrix}
\Omega_{1,1}^{N_{M,A}-1} & \Omega_{1,1}^{N_{M,A}-2} & \cdots & 1 & \frac{(-1)^1 P_A(\Omega_{1,1})P_B(\Omega_{1,1})}{F_{C,A}(\Omega_{1,1})E_B(\Omega_{1,1})} & 0 \\
\Omega_{1,2}^{N_{M,A}-1} & \Omega_{1,2}^{N_{M,A}-2} & \cdots & 1 & \frac{(-1)^2 P_A(\Omega_{1,2})P_B(\Omega_{1,2})}{F_{C,A}(\Omega_{1,2})E_B(\Omega_{1,2})} & 0 \\
\vdots & \vdots & \vdots & \vdots & & \\
\Omega_{1,N_{1,T}+1}^{N_{M,A}-1} & \Omega_{1,N_{1,T}+1}^{N_{M,A}-2} & \cdots & 1 & \frac{(-1)^{N_{1,T}+1} P_A\left(\Omega_{1,N_{1,T}+1}\right)P_B\left(\Omega_{1,N_{1,T}+1}\right)}{F_{C,A}\left(\Omega_{1,N_{1,T}+1}\right)E_B\left(\Omega_{1,N_{1,T}+1}\right)} & 0 \\
\Omega_{2,1}^{N_{M,A}-1} & \Omega_{2,1}^{N_{M,A}-2} & \cdots & 1 & 0 & \frac{(-1)^1 P_A(\Omega_{2,1})P_B(\Omega_{2,1})}{F_{C,A}(\Omega_{2,1})E_B(\Omega_{2,1})} \\
\Omega_{2,2}^{N_{M,A}-1} & \Omega_{2,2}^{N_{M,A}-2} & \cdots & 1 & 0 & \frac{(-1)^2 P_A(\Omega_{2,2})P_B(\Omega_{2,2})}{F_{C,A}(\Omega_{2,2})E_B(\Omega_{2,2})} \\
\vdots & \vdots & \vdots & \vdots & & \\
\Omega_{2,N_{2,T}+1}^{N_{M,A}-1} & \Omega_{2,N_{2,T}+1}^{N_{M,A}-2} & \cdots & 1 & 0 & \frac{(-1)^{N_{2,T}+1} P_A\left(\Omega_{2,N_{2,T}+1}\right)P_B\left(\Omega_{2,N_{2,T}+1}\right)}{F_{C,A}\left(\Omega_{2,N_{2,T}+1}\right)E_B\left(\Omega_{2,N_{2,T}+1}\right)}
\end{bmatrix}
\begin{bmatrix} f_{2,A} \\ f_{3,A} \\ \vdots \\ f_{N_{M,A}} \\ \Delta_1 \\ \Delta_2 \end{bmatrix}$$

$$= \begin{bmatrix}
\frac{(-1)^{N_{DB,A}}\varepsilon_{r,A}F_B(\Omega_{1,1})E^*_A(\Omega_{1,1})}{\varepsilon_{r,B}F_{C,A}(\Omega_{1,1})E_B(\Omega_{1,1})} - \Omega_{1,1}^{N_{M,A}} \\
\frac{(-1)^{N_{DB,A}}\varepsilon_{r,A}F_B(\Omega_{1,2})E^*_A(\Omega_{1,2})}{\varepsilon_{r,B}F_{C,A}(\Omega_{1,2})E_B(\Omega_{1,2})} - \Omega_{1,2}^{N_{M,A}} \\
\vdots \\
\frac{(-1)^{N_{DB,A}}\varepsilon_{r,A}F_B\left(\Omega_{1,N_{1,T}+1}\right)E^*_A\left(\Omega_{1,N_{1,T}+1}\right)}{\varepsilon_{r,B}F_{C,A}\left(\Omega_{1,N_{1,T}+1}\right)E_B\left(\Omega_{1,N_{1,T}+1}\right)} - \Omega_{1,N_{1,T}+1}^{N_{M,A}} \\
\frac{(-1)^{N_{DB,A}}\varepsilon_{r,A}F_B(\Omega_{2,1})E^*_A(\Omega_{2,1})}{\varepsilon_{r,B}F_{C,A}(\Omega_{2,1})E_B(\Omega_{2,1})} - \Omega_{2,1}^{N_{M,A}} \\
\frac{(-1)^{N_{DB,A}}\varepsilon_{r,A}F_B(\Omega_{2,2})E^*_A(\Omega_{2,2})}{\varepsilon_{r,B}F_{C,A}(\Omega_{2,2})E_B(\Omega_{2,2})} - \Omega_{2,2}^{N_{M,A}} \\
\vdots \\
\frac{(-1)^{N_{DB,A}}\varepsilon_{r,A}F_B(\Omega_{1,2})E^*_A\left(\Omega_{2,N_{2,T}+1}\right)}{\varepsilon_{r,B}F_{C,A}\left(\Omega_{2,N_{2,T}+1}\right)E_B\left(\Omega_{2,N_{2,T}+1}\right)} - \Omega_{2,N_{2,T}+1}^{N_{M,A}}
\end{bmatrix} \tag{18}$$

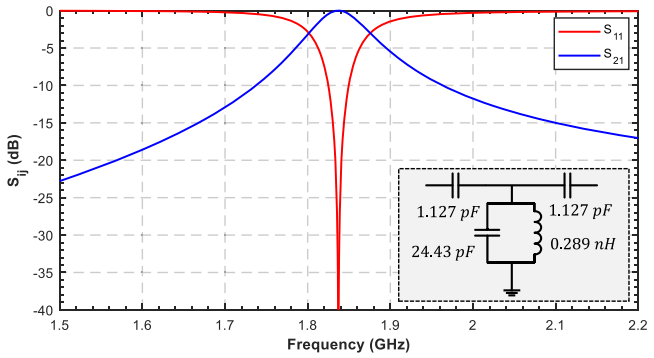

Fig. 6. Reference $Z_L(f)$ used throughout Sections IV and V.

considering only the RZs of S_A in S_T follows a procedure similar to that outlined in Section III-A. In this case, (18) is modified so that the algorithm searches for $N_{M,A}$ in-band RZs in the S_T response, rather than the actual $N_{M,T}$ RZs. This is achieved by reducing the number of rows in (18) from $N_{M,T}+2$ to $N_{M,A}+2$, resulting in a system of equations that is no longer overdetermined. In addition, *step 6* from Section III-A must be carefully revised, since there are still $N_{M,T}+2$ extrema points, but $N_{M,T}-N_{M,A}$ of them should be removed. The extrema points to be removed are those located outside the passband.

C. Convergence of the Algorithm

The Remez-like algorithms presented in Sections III-A and III-B typically converge to a stable solution in less than ten iterations. However, as explained in [8], DB coefficient-based approaches tend to generate highly clustered RZs, leading to excessively large coefficients and numerical inaccuracies for $FBW < 4\%$ or $N > 7$, due to the limited precision of double-precision arithmetic. These limitations can be addressed using extended-precision tools, such as Advanpix [25], at the expense of increased computational time, or by root-finding techniques, which iteratively compute the roots of the polynomial equations while keeping numerical values within a manageable range, enabling filter orders up to 18 regardless of the FBW [8], [9], [26].

IV. Filter Behavior When $Z_L(f)$ and Its RZs Are Included in S_T

This section addresses several key aspects involved in matching a filter to a $Z_L(f)$, including its RZs in S_T. The flexibility of the proposed method is analyzed in terms of the achievable RL level, considering that, as established by Fano [14] and Martinez [17], not all filtering functions can be perfectly matched to arbitrary impedances. As expected, evaluating the method for the infinite variety of possible $Z_L(f)$ cases is unfeasible. Therefore, a single representative example is used throughout this section to discuss the different synthesis aspects related to the RL level. Fig. 6 presents the response and circuit of the $Z_L(f)$, whose rational function S_B is obtained by means of vector fitting [19]. A fifth-order ladder filter synthesized for the 1810–1870-MHz band is used for the analysis.

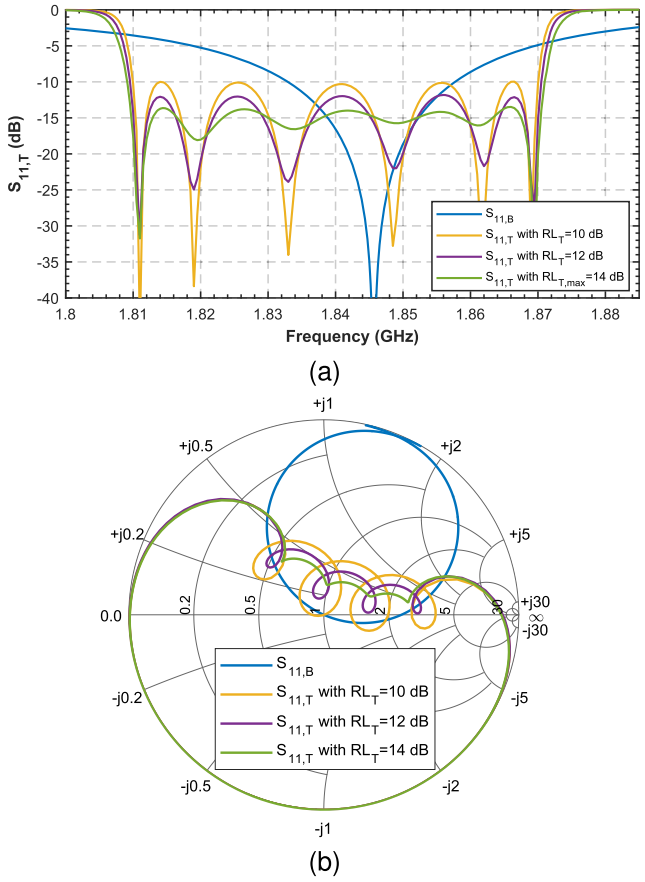

Fig. 7. Fifth-order ladder filter designed for different RL_T levels up to the $RL_{T,\max}$. (a) $S_{11,T}$ response for the different RL_T levels. (b) Smith chart representation of $S_{22,A}$ and $S^*_{11,B}$.

A. Flexibility in Setting the RL_T Level

The method proposed in this work offers flexibility in setting the RL_T level of the cascaded response S_T. This introduces an additional degree of freedom in the design process, since the solution with the best RL is not always the most optimal in terms of technological feasibility or OoB rejection [5]. For instance, in the design of AW ladder filters, it is common to seek evenly distributed k_t^2 values across all AW resonators, enabling their fabrication on a single die using the same piezoelectric material without external elements. As demonstrated in [5] and [23], it is possible to identify an RL level that allows convergence to a solution where all resonators share the same k_t^2. Therefore, having the freedom to control RL during the synthesis significantly facilitates the fulfillment of stringent OoB rejection specifications and technological constraints.

Fig. 7(a) demonstrates how the response S_T of four different filters designed to cover the 1810–1870-MHz frequency span is obtained with different RL_T levels. Furthermore, Fig. 7(b) shows how the reflection coefficient $S_{11,A}$ oscillates around the complex conjugated $S^*_{11,B}$ network with different amplitudes depending on the target RL_T level. Unlike the classical generalized Chebyshev response, where the impedance locus crosses 50 Ω at each RZ, in this case, the impedance locus of $S_{11,A}$ does not necessarily cross $S^*_{11,B}$ at the RZ frequencies, since they are now complex. This occurs for all RZs except

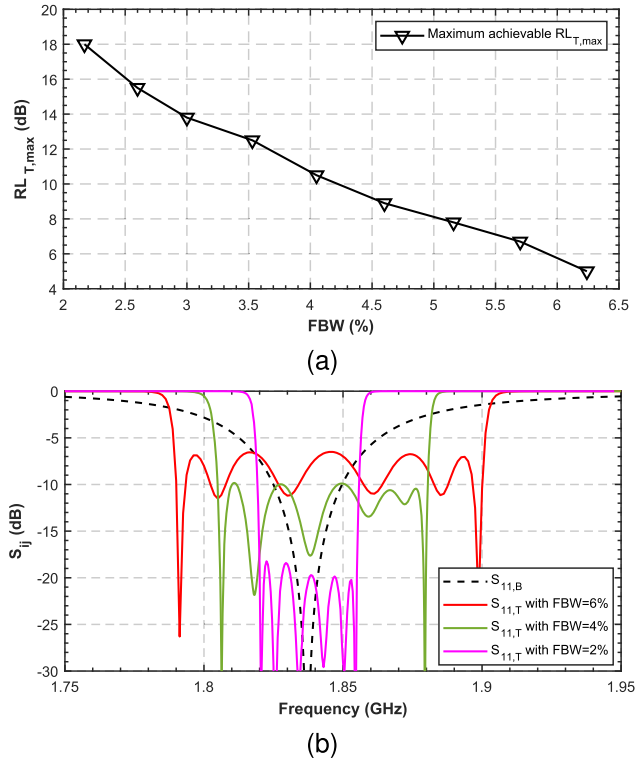

Fig. 8. Influence of the FBW on the $RL_{T,\max}$. (a) FBW as a function of $RL_{T,\max}$. (b) Representation of $Z_L(f)$ and the resulting $S_{11,T}$ for three different FBWs synthesized with the $RL_{T,\max}$.

the first and the last, because, as shown in Fig. 7(b), $S_{11,A}$ always intersects $S^*_{11,B}$ at both the beginning and the end of the passband, which makes these particular RZs purely real, as illustrated in Fig. 7(a).

Each S_T is obtained by cascading the synthesized fifth-order ladder filter S_A with the fixed second-order S_B of Fig. 6 to obtain the four RL_T levels. Note how, as the RL_T increases, the S_T response tends to exhibit a behavior closely resembling that of a bounded Chebyshev filter [17], [18], which indicates proximity to the Bode–Fano limit. In this case, the maximum achievable return loss ($RL_{T,\max}$) is around 10 dB, and beyond this physical limit, the proposed Remez-like algorithm will no longer converge.

B. Influence of the FBW in the Achievable $RL_{T,Max}$

When part of the filtering function must remain fixed, a significant constraint is introduced during the synthesis of the characteristic polynomials. This is the case for S_A filters that aim to construct an equiripple overall response S_T while targeting a $Z_L(f)$. In such scenarios, only S_A is under design control, meaning that the achievable performance of S_T is significantly more limited. As demonstrated by Fano [14], the load network $Z_L(f)$, together with the FBW, imposes a fundamental limit on the $RL_{T,max}$ level. In particular, the higher the FBW, the lower the achievable $RL_{T,\max}$. To validate this assumption using the methodology proposed in Section III-A, Fig. 8(a) shows the achievable $RL_{T,\max}$ of S_T as a function of FBW, using the same S_B in all cases. In addition, Fig. 8(b) illustrates three of these filters in which S_A is synthesized

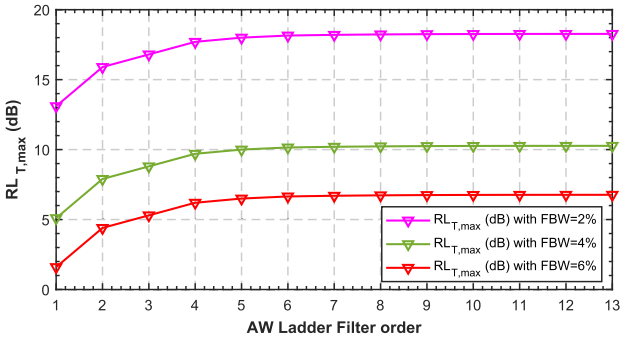

Fig. 9. $RL_{T,\max}$ for a ladder filter designed with different filter orders N.

to achieve $RL_{T,\max}$ in S_T. As expected, as the FBW of S_A increases, the $RL_{T,\max}$ of S_T decreases.

C. Influence of the S_A Filter Order in the Achievable $RL_{T,Max}$

Apart from the FBW and the $Z_L(f)$ network, another parameter that influences the achievable $RL_{T,\max}$ level is the order of S_A. As demonstrated in [17], the higher the filter order of S_A, the higher the achievable $RL_{T,\max}$. However, this relationship is not linear, since $RL_{T,\max}$ approaches a horizontal asymptote as the order of S_A increases.

This behavior is validated in Fig. 9, where ladder filters of different orders are synthesized using the methodology proposed in Section III-A. It can be observed that the $RL_{T,\max}$ values required to achieve a quasi-equiripple response increase with the filter order. However, beyond approximately order 6, this improvement starts to slow down exponentially. Let us highlight that the order N that appears in Fig. 9 refers to the number of resonators, rather than the order $N_{DB,A}$, which defines the order of the DB filtering function of S_A. This observation is consistent with the results reported by Helton [16], which demonstrated that achieving a filter whose impedance is exactly the complex conjugate of $Z_L(f)$ over the entire passband would require characteristic polynomials of infinite order, or equivalently, an infinite number of resonators. In such a case, a perfectly flat RL_T with a level approaching ∞ dB could be obtained. However, this situation represents a purely theoretical limit and is not physically realizable.

D. Impact of the Imaginary RZs of S_A on S_T

As explained in [8], the two $j\Omega_{RZ,A}$ that model the frequency-dependent input and output phases also determine the values of the first and last elements in the ladder filter. In contrast to [8], where the $j\Omega_{RZ}$ must appear in complex-conjugate pairs due to the symmetry properties imposed by the logarithmic mapping function, the formulation presented in Sections II and III-A allows for the asymmetric placement of the two $j\Omega_{RZ,A}$, introducing an additional degree of freedom for the ladder filter design, as shown in Fig. 5. In fact, this asymmetry becomes essential when matching the filter to a given $Z_L(f)$, since the two $j\Omega_{RZ,A}$ play a distinct role in the cascaded response S_T.

On one hand, the negative $-j\Omega_{RZ,A}$ is responsible for modeling the input phase of $S_{11,A}$ and $S_{11,T}$. As illustrated

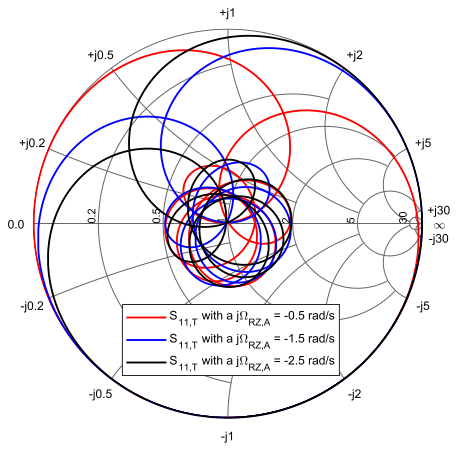

Fig. 10. Influence of the negative $j\Omega_{RZ,A}$ on the input phase orientation of the S_T locus impedance.

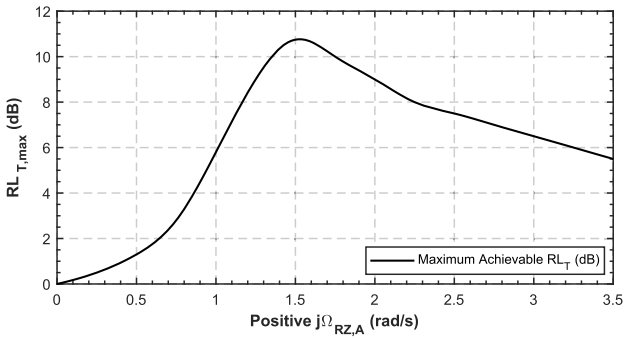

Fig. 11. Influence of the positive $j\Omega_{RZ,A}$ on $RL_{T,\max}$.

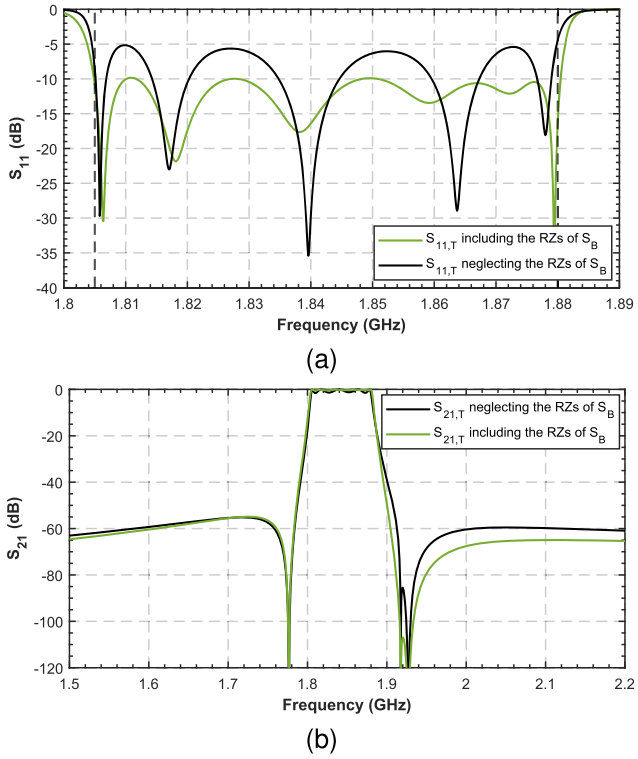

Fig. 12. Differences between including and neglecting the contribution of the RZs of S_B in the synthesized S_T. (a) Maximum achievable $RL_{T,max}$. (b) Transmission responses.

in Fig. 10, varying the position of this $-j\Omega_{RZ,A}$ produces a rotation of the Chebyshev-like ripple pattern of $S_{11,T}$ around the source impedance at 50 Ω without affecting the magnitude, neither the $RL_{T,\max}$ level. This behavior is also expected to occur from the perspective of the load of $S_{22,B}$ and $S_{22,T}$, where this time, the positive $+j\Omega_{RZ,B}$ would play an analogous role. However, in this work, S_B is considered fixed and therefore cannot be tuned. Furthermore, the $-j\Omega_{RZ,A}$ is particularly useful for ensuring that the filtering function of S_A can be embedded inside the ladder filter topology, thereby preserving the expected S_A response with $Z_S = Z_L = 50\ \Omega$. As discussed in [8], when the filtering function is asymmetric ($\angle S_{11,A} \neq \angle S_{22,A}$), it may not always be possible to achieve a Z_L of 50 Ω when extracting the ladder topology from S_A, since the admittance after the last partial extraction might differ from unity.

On the other hand, the positive $+j\Omega_{RZ,A}$ models the output phase of $S_{22,A}$. In addition, this parameter is also responsible for controlling the optimum $RL_{T,\max}$ of the S_T response. In other words, it determines the rotation of the ripple pattern of $S_{22,A}$ around $S_{11,B}$, and this orientation should be the complex conjugate of $S_{11,B}$. Fig. 11 illustrates how $RL_{T,\max}$ varies with the position of the $+j\Omega_{RZ,A}$ in a fifth-order ladder filter. The optimal value occurs at $j\Omega_{RZ,A,\text{Optim}} = 1.5$, where RL_T reaches the minimum level for this $Z_L(f)$. Consequently, the position of $+j\Omega_{RZ,A}$, together with the RL level, is of critical importance, as it determines how far the Bode–Fano limit can be approached.

V. Filter Behavior When $Z_L(f)$ Is Included in S_T but Its RZs Are Excluded From the Equiripple

Up to this point, this work has considered cases in which the RZs of $Z_L(f)$ lie within the passband of S_T. This section compares how the $RL_{T,max}$ of a suboptimal solution is reduced when S_A only oscillates around S_B without involving its RZs in the quasi-equiripple of S_T.

A. Differences Between Including and Neglecting the Contribution of the RZs of S_B in the Synthesized S_T

Fig. 12 reproduces the same example as Fig. 7(a), but using the methodology described in Section III-B to exclude the RZ of S_B from S_T. Interestingly, the differences between including and neglecting the contribution of the RZs of S_B in the synthesized S_T resemble that of a reduced Chebyshev filtering function with one or more RZs shifted into the complex plane [27]. As explained in [27], for each RZ moved to the complex plane, the OoB rejection of the filter behaves as that of a lower-order network [see Fig. 12(b)]. In this case, the RZ lying in the complex plane corresponds to one of the S_B that is not being considered. For this reason, the $RL_{T,max}$ is always lower than when the RZs of S_B are included in S_T, since the Bode–Fano limit cannot be reached without them.

Nevertheless, neglecting the RZs of S_B offers the possibility of achieving a suboptimal response when the $Z_L(f)$ cannot be tuned, and its RZs lie outside the passband.

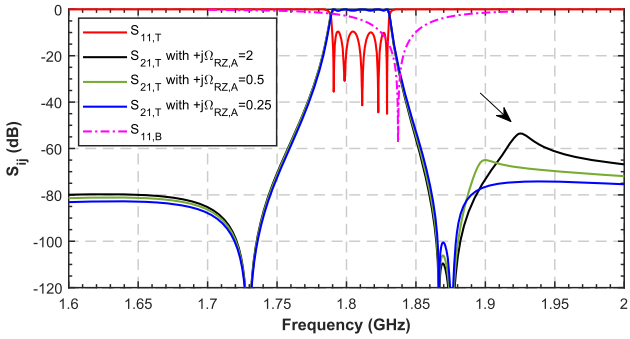

Fig. 13. Fifth-order ladder filter synthesized excluding the far-band RZ of S_B, leading to undesired spikes that can be controlled adjusting $+j\Omega_{RZ,A}$.

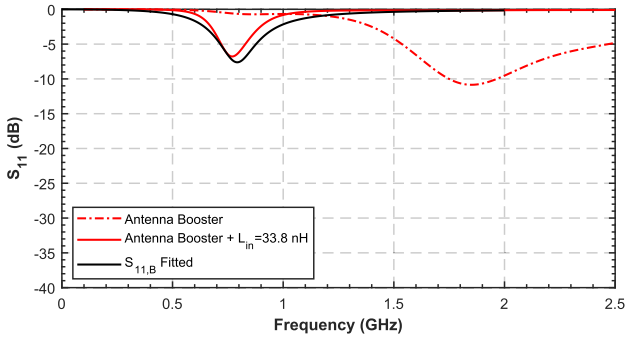

Fig. 14. Reflection response comparison of the antenna booster without the series inductor, with the series inductor, and with the fitted model of the latter configuration.

B. Matching the Filter Neglecting the RZs of S_B: Appearance of Spurious Spikes in the Transmission Response of S_T

As explained in [28] and [29], cascading different networks can trigger the appearance of spurious resonances, observed as sharp spikes in the transmission response. This undesired behavior is understood as a strong mismatch that occurs when $\angle S_{22,A} = \angle - S_{11,B}$ is satisfied in the OoB region, that is, when the denominator of (10), (12), and (14) becomes zero. Moreover, Acosta et al. [29] demonstrated that the position of the spike can be relocated to a region where it is suppressed by adjusting the input phase of $F(s)$ in the LP domain.

The appearance of these spikes can also be understood from another perspective: when not considering $Z_L(f)$ in the cascaded response S_T, the RZs associated with S_B shift in frequency in an uncontrolled manner, causing the appearance of spurious transmission spikes. Fig. 13 shows the response of a fifth-order ladder filter that, instead of being synthesized from 1810 to 1870 MHz, that is, around the RZ of S_B located at 1837 MHz, is designed for the 1750–1800-MHz band using the methodology described in Section III-B. In this situation, a spurious spike appears at 1925.7 MHz. Similar to [29], this spike can be relocated by adjusting the positive $+j\Omega_{RZ,A}$ of S_A, as represented in Fig. 13. This demonstrates that $+j\Omega_{RZ,A}$ also controls the spike position when the RZ of S_B is located outside the passband by controlling the output phase.

VI. Validation Examples

To validate the effectiveness of the proposed methodology, two case studies with distinct filter topologies and $Z_L(f)$ are presented. In the first case, a wideband third-order all-pole filter is synthesized and compared with a fabricated prototype, where a real antenna serves as $Z_L(f)$, characterized by a strong impedance variation. The RZ of this $Z_L(f)$ is included in the S_T response. In the second case, a narrowband fifth-order AW ladder filter is synthesized using the Menlo Microsystems MM5140 switch [30] as $Z_L(f)$, which exhibits a smooth impedance variation. The RZs of this $Z_L(f)$ are neglected in the S_T response.

A. Third-Order All-Pole Filter Matched to an Antenna Booster

This example aims to demonstrate the validity of the proposed methodology for all-pole topologies. In this case, an all-pole filter is selected for experimental validation over the 700–960-MHz frequency range. The filter is designed to be matched to an antenna booster [31], [32] with the objective of approaching the Bode–Fano limit. The antenna booster consists of an electrically small, nonresonant element in which the operating frequencies can be tuned by adjusting the matching network and by properly positioning the antenna booster on the printed circuit board (PCB), rather than modifying the antenna geometry. In the proposed experiment, the matching network is interpreted as a third-order all-pole filter synthesized considering the contribution of the antenna booster's RZ.

First, the $S_{11,B}$ parameter of the antenna booster is measured without the matching network, and depicted in Fig. 14. Since the antenna booster has its RZ at 1.75 GHz, a 33.829-nH inductor is used to shift it down into the passband, from 700 to 960 MHz. At this point, the vector fitting technique of [19] is used for modeling this $Z_L(f)$ using a second-order filtering function. However, it must be noted that the proposed methodology relies on cascading two-port networks, whereas antennas are typically measured as one-port devices. This discrepancy can be addressed by defining a fictitious transmission parameter $S_{12,B} = S_{21,B}$ based on the S-parameter formulation introduced by Kurokawa [33], such that

$$[S_B]^{(2\text{-port})} = \begin{bmatrix} S_{11,B}(f) & S_{12,B}(f) \\ S_{21,B}(f) & S_{22,B}(f) \end{bmatrix} \tag{25}$$

$$= \begin{bmatrix} \frac{Z_L(f)-Z_S}{Z_S^*+Z_L(f)} & \frac{2\sqrt{\Re\{Z_S\}\Re\{Z_L(f)\}}}{Z_S+Z_L(f)} \\ \frac{2\sqrt{\Re\{Z_S\}\Re\{Z_L(f)\}}}{Z_S+Z_L(f)} & \frac{Z_S-Z_L^*(f)}{Z_S+Z_L(f)} \end{bmatrix} \tag{26}$$

where $Z_S = 50\ \Omega$ and

$$Z_L(f) = Z_0 \cdot \frac{1+S_{11,B}^{(1\text{-port})}}{1-S_{11,B}^{(1\text{-port})}}. \tag{27}$$

The resulting S_B polynomials, normalized to $f_{c2} = 960$ MHz, are the following ones:

$$P_B(s) = s^2 + 25.116s + 0.6859$$
$$F_B(s) = -s^2 + 0.1948s - 0.6213$$
$$E_B(s) = s^2 + 0.4242s + 0.6213$$
$$\varepsilon_B = 59.2117$$

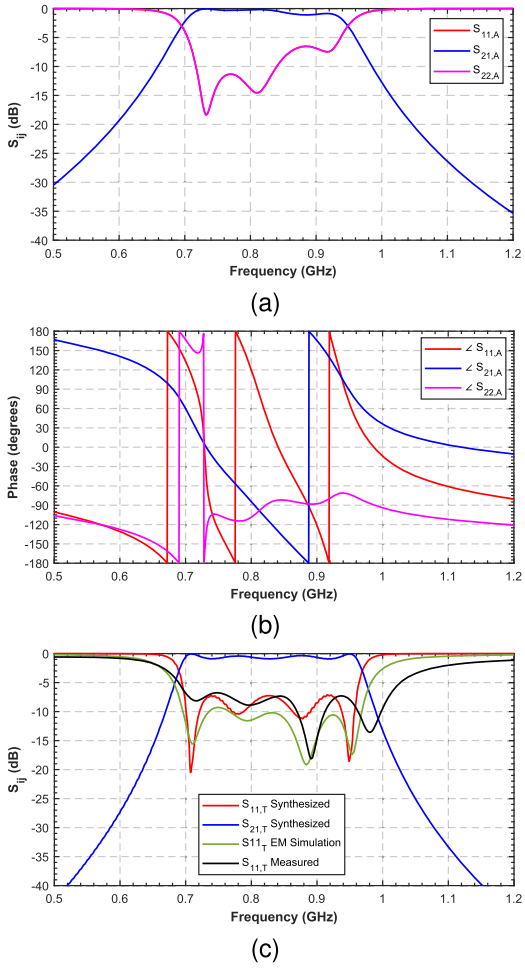

Fig. 15. S parameters of (a) synthesized S_A magnitude, (b) synthesized S_A phase, and (c) cascaded S_T, including simulated and fabricated responses.

$$\varepsilon_{r,B} = 1.0001.$$

In addition, Fig. 14 compares the obtained S_B polynomials with the original response. Note that the fit response is not exact when using this second-order function, because the antenna's Touchstone file includes parasitic effects that increase the actual order of the filtering function. Although the fit is not exact, the model is sufficiently accurate to obtain a set of characteristic polynomials of $Z_L(f)$ very close to the real ones, without excessively overdetermining the system of equations in (18).

To achieve a quasi-equiripple S_T response at the Bode–Fano limit using a third-order all-pole filter ($N_{DB,A} = 8$) with $\Omega_{TZ} = [0, 0, 0]$, a target $RL_T = 8$ dB, and a $+j\Omega_{RZ,A} = 0.36$ rad/s are required. In addition, as explained in Section IV-D, a value of $-j\Omega_{RZ,A} = 0.39$ rad/s is chosen to extract the ladder topology from S_A without altering the 50-Ω load termination. After solving the system of equations of (18) using the Remez-like algorithm explained in Section III-A, the resulting S_A distorted polynomials are

$$P_A(s) = s^3$$
$$F_A(s) = s^8 - 0.1343s^7 + 2.091s^6 - 0.2022s^5 + 1.3134s^4 - 0.0803s^3 - 0.1599s^2 - 0.0042s - 0.0542$$
$$E_A(s) = s^8 + 1.0548s^7 + 2.6383s^6 + 2.2020s^5 + 2.3148s^4 + 1.4668s^3 + 0.7416s^2 + 0.3126s + 0.0542$$
$$\varepsilon_A = 126.6794$$
$$\varepsilon_{r,A} = 1.$$

TABLE I
EXTRACTED ELEMENTS OF THE THIRD-ORDER ALL-POLE FILTER MATCHED TO THE ANTENNA BOOSTER

Resonator	C (pF)	L (nH)	In-band Smith Chart Plot
1 (SE)	3.945	14.223	
2 (SH)	55.508	0.690	
3 (SE)	2.507	19.759	
Input Element	5.521	No	
Output Element	7.191	33.829	

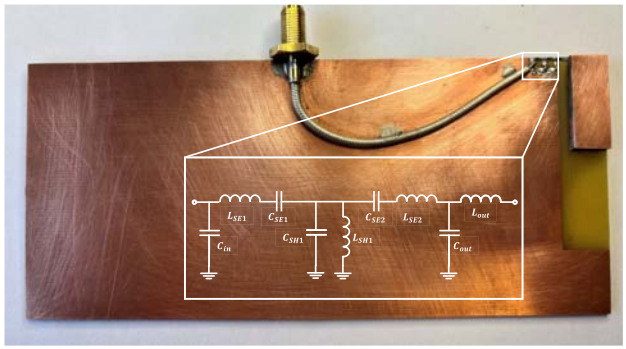

Fig. 16. Picture of the third-order all-pole filter matched to the antenna booster.

Fig. 15(a) shows the corresponding S_A response. These S_A polynomials are used to extract the elements of the all-pole filter topology, which are represented in Table I. Notice that when a $Z_L(f)$ is considered, the RZs are shifted into the complex plane, which causes the phases of $S_{11,A}$ and $S_{22,A}$ to differ in Fig. 15(b) and, consequently, makes the elements of the all-pole filter asymmetric.

Fig. 15(c) shows the S_T response obtained after cascading S_A and S_B, compared with simulated and fabricated prototype. Since S_B was approximated as a second-order function, it does not perfectly represent the actual $Z_L(f)$, leading to a slight degradation of the quasi-equiripple response from the expected $RL_T = 8$ dB to $RL_T = 7.3$ dB. Nevertheless, despite the inherent modeling limitations of the real $Z_L(f)$, the all-pole filter was synthesized very close to the Bode–Fano limit. These results demonstrate that the proposed methodology allows for a much faster exploration of different filtering functions and topologies compared to traditional optimization processes, even when real $Z_L(f)$ devices are considered.

Fig. 16 shows the fabricated antenna booster, which measures $12 \times 3 \times 2.4$ mm^3 (height) and is mounted on a 120×60 mm^2 ground plane printed on an FR4 substrate with a thickness of 1 mm, relative permittivity $\varepsilon_r = 4.15$, and loss tangent $\tan\delta = 0.017$. The overall PCB dimensions

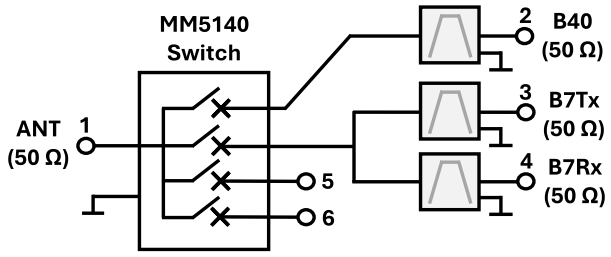

Fig. 17. Schematic of the proposed fictitious setup used to synthesize a Band 40 fifth-order AW ladder filter matched to an MM5140 switch, including a Band 7 duplexer connected through another switch port.

are 131 × 60 mm. The all-pole filter is implemented using surface-mount device (SMD) inductors and capacitors. Let us highlight that the main cause of the bandwidth widening in Fig. 15(c) is the use of SMD components whose nominal values are selected to achieve the desired response at the passband center frequency. However, since the filter operates over a broadband range, the nominal values of the SMDs vary, particularly near the band edges. This issue could be mitigated by using a different technology with better tolerances or simply by employing higher-quality SMD components.

B. Fifth-Order AW Ladder Filter Matched to an MM5140 Switch

In this example, a fifth-order AW ladder filter is synthesized to match a real Menlo Microsystems MM5140 switch device over the Band 40 (2300–2400 MHz) frequency range. The corresponding Touchstone files were obtained from [30] and it should be noted that the authors of this work do not know anything about its reactive model. To create a more realistic experimental setup, a fictitious Band 7 duplexer (2500–2570 MHz uplink and 2620–2690 MHz downlink) is connected through one of the two switch ports set to the ON state, as represented in Fig. 17. In this configuration, port 1 corresponds to the antenna port, port 2 to the AW ladder filter input, and port 3 to the duplexer, which is included only to reproduce the loading effects that are usually present in real front-end modules. To highlight the purpose of this work, the duplexer has been intentionally designed without accounting for any loading effects, whereas the AW ladder filter has been synthesized while fully considering them.

Fig. 18(a) shows the S parameters of the synthesized Band 7 duplexer with RL = 15 dB using the methodology of [34], which is constrained to 50-Ω source and load terminations. Then, Fig. 18(b) shows the same duplexer connected to the actual switch device, with port 2 in state OFF. At this point, it can be observed that the switch impedance, which deviates from a constant 50 Ω, slightly degrades the expected behavior of the duplexer from RL = 15 dB to RL = 11 dB due to impedance mismatch.

Fig. 18(c) depicts the $S_{11,B}$, $S_{22,B}$, and $S_{21,B}$ parameters, taking into account the loading effects introduced by both the switch and the duplexer. This figure also shows the fit response obtained using a sixth-order filtering function. As expected, this order is insufficient to accurately model the entire frequency spectrum of such a complex impedance.

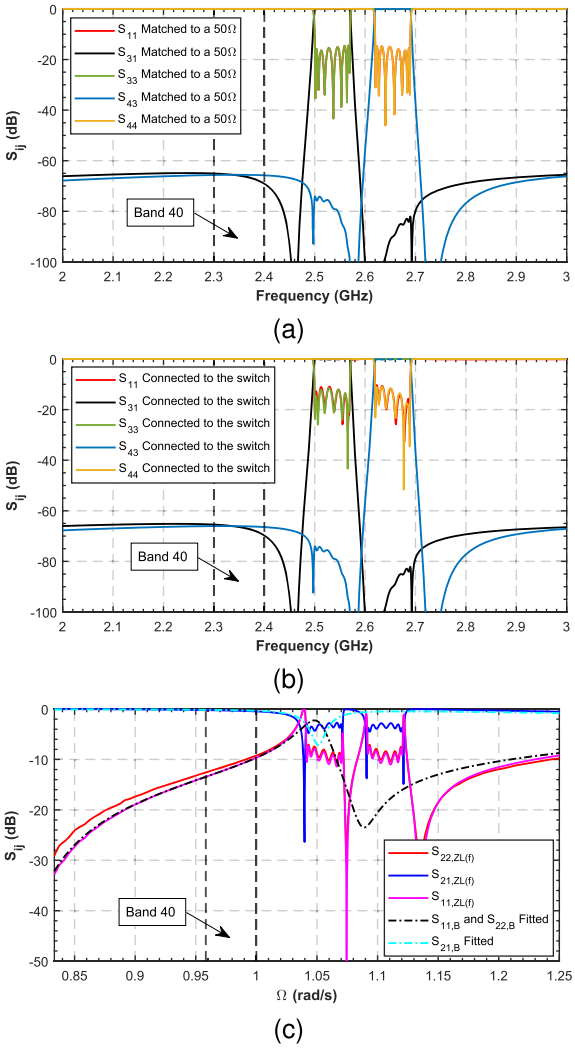

Fig. 18. S parameters of (a) synthesized duplexer matched to 50-Ω source and load terminations, (b) same duplexer when switch port 2 is set to off, and (c) real $Z_L(f)$ response evaluated with ports 2 and 3 set to on, compared with the fit S_B response.

However, by applying weighting to the passband, the $S_{22,B}$ fit model achieves adequate accuracy within the frequency range of interest. Note that $S_{11,B}$ is not accurately modeled within the frequency range of interest because its magnitude differs from that of $S_{22,B}$ due to the dissipative losses. As a result, the vector fitting procedure requires different normalization constants for $S_{11,B}$ and $S_{22,B}$ to ensure a common denominator polynomial. Consequently, just one of these two normalization constants is selected. As a result, the system of equations in (18) is no longer suitable for solving $F(s)$ and $F^*(s)$ simultaneously, ensuring a quasi-equiripple response only in one of them. In this example, $S_{22,B}$ is selected for accurate fitting, obtaining the following S_B polynomials:

$$P_B(s) = s^6 - 4.616s^5 + 7.107s^4 - 33.612s^3 + 6.185s^2 - 31.569s - 0.202$$

$$F_B(s) = s^6 - 7.859s^5 + 20.584s^4 - 14.620s^3 + 35.511s^2 - 6.465s + 14.791$$

$$E_B(s) = s^6 + 7.009s^5 + 18.559s^4 + 32.886s^3 + 27.766s^2$$

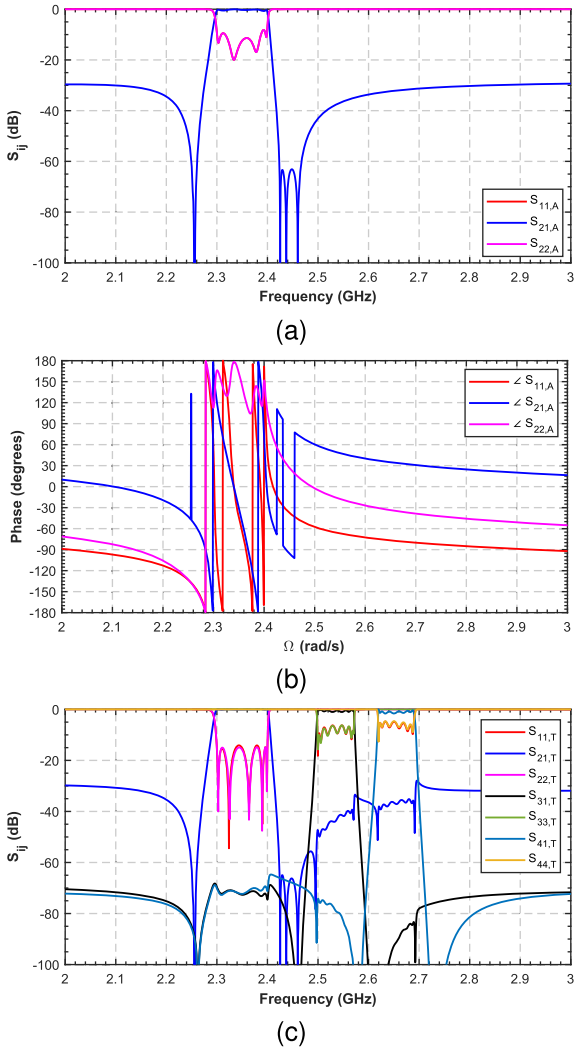

Fig. 19. S parameters of (a) fifth-order AW ladder filter magnitude, (b) fifth-order AW ladder filter phase, and (c) overall response S_T.

TABLE II
AW ELEMENTS OF THE SYNTHESIZED FIFTH-ORDER LADDER FILTER

Resonator	C_{stat} (pF)	f_s (MHz)	k_t^2 (%)	In-band Smith Chart Plot
1 (SE)	0.770	2371.9	8.5	
2 (SH)	4.494	2256.5	8.5	
3 (SE)	0.709	2350.8	8.5	
4 (SH)	4.161	2255.3	8.5	
5 (SE)	2.232	2338.7	8.5	
L_{in} (nH)	4.800	L_{out} (nH)	6.532	

$$+ 27.644s + 8.922$$
$$\varepsilon_B = 1.2536$$
$$\varepsilon_{r,B} = 1.6583.$$

To synthesize the fifth-order AW ladder filter S_A, corresponding to a filter order of $N_{DB,A} = 12$ in the DB domain, the following configuration of normalized TZs and $j\Omega_{RZ,A}$ is chosen: $\Omega_{TZ} = [1.0105, -1.0105, 0.9397, -0.9397, 1.0155, -1.01550.9402, -0.9402, 1.0250, -1.0250, 0]$, and $j\Omega_{RZ,A} = [-1.05, +1.8]$ designed for an $RL_T = 15$ dB. After applying the Remez-like algorithm of Section III-B for solving (18), the resulting S_A polynomials are

$$P_A(s) = s^{12} + 4.8700s^{10} + 9.4728s^8 + 9.1993^6 + 4.4600s^4 + 0.8636s^2$$
$$F_A(s) = s^{12} - 0.7772s^{11} + 2.9420s^{10} - 3.6619s^9 + 0.2436s^8 - 6.8972s^7 - 8.4791s^6 - 6.4919s^5 - 12.4784s^4 - 3.0534s^3 - 7.2548s^2 - 0.5741s - 1.5572$$
$$E_A(s) = s^{12} + 2.9449s^{11} + 6.9703s^{10} + 14.2672s^9 + 19.3916s^8 + 27.6324s^7 + 27.9117s^6 + 26.7430s^5 + 22.0870s^4 + 12.9335s^3 + 9.1538s^2 + 2.5005s + 1.5572$$
$$\varepsilon_A = 9.3022$$
$$\varepsilon_{r,A} = 1.$$

Fig. 19(a) and (b) illustrates the S_A response corresponding to the obtained characteristic polynomials. Table II summarizes the circuit elements extracted from S_A using the DB methodology presented in [8]. In addition, Fig. 19(c) shows the S_T response obtained after cascading S_A with the real $Z_S(f)$, demonstrating that the proposed methodology achieves the expected in-band quasi-equiripple response at $RL_T = 15$ dB. In contrast, the duplexer synthesized with 50-Ω terminations is now degraded not only by the mismatch with the switch, as already observed in Fig. 18(a), but also by the loading effects introduced by the AW ladder filter when port 2 is on. This poor performance in the duplexer arises because the ladder filter does not enforce an open circuit across the frequency span of the duplexer bands, as shown in Fig. 19(b). Although Giménez et al. [5] demonstrated that it is possible to impose an open circuit by adjusting the phase of the polynomial $F(s)$ using the $-j\Omega_{RZ,A}$, this result assumes that the filter is synthesized with constant source and load impedances. When the filter must be synthesized considering a fixed $Z_S(f)$, an additional constraint is introduced that also depends on the input phase of the filter. To match the filter to the $Z_S(f)$, the input phase must simultaneously satisfy two conditions: rotate the Chebyshev-like ripple pattern of the filter to align it with the $Z_S^*(f)$ and create an open circuit at the tail of the phase on the Smith chart. Achieving both conditions simultaneously with the same $-j\Omega_{RZ,A}$ is extremely challenging, resulting in a tradeoff that the designer must consider: either allow some mismatch to improve the open-circuit behavior in the duplexer bands, or accept a less ideal open circuit to preserve the equiripple.

VII. CONCLUSION

This work has presented a numerical Remez-based methodology for synthesizing filters or matching networks to any $Z_L(f)$ while directly controlling the RL level of the cascaded response S_T. This approach not only enables the synthesis of the most optimal response by accounting for the RZs of $Z_L(f)$, but also supports the design of suboptimal responses

when those RZs lie outside the passband and the $Z_L(f)$ cannot be tuned. The study analyzes both cases in depth, providing a comprehensive view of the parameters that determine the maximum achievable return loss in S_T. This study has highlighted how bandwidth, phase, filter order, and load characteristics fundamentally limit the maximum achievable $RL_{T,max}$ in S_T. Two case studies involving real devices have confirmed the effectiveness and generality of the approach: a wideband third-order filter matched to an antenna booster, and a fifth-order AW ladder filter matched to a Menlo Microsystems MM5140 switch. Together, these results demonstrate that the proposed methodology provides a robust and systematic framework for early-stage RF front-end design under realistic, frequency-dependent loading conditions.

REFERENCES

[1] A. Hagelauer et al., "From microwave acoustic filters to millimeter-wave operation and new applications," *IEEE J. Microw.*, vol. 3, no. 1, pp. 484–508, Jan. 2023.

[2] A. Hagelauer, G. Fattinger, C. C. W. Ruppel, M. Ueda, K.-Y. Hashimoto, and A. Tag, "Microwave acoustic wave devices: Recent advances on architectures, modeling, materials, and packaging," *IEEE Trans. Microw. Theory Techn.*, vol. 66, no. 10, pp. 4548–4562, Oct. 2018.

[3] R. Ruby, "A snapshot in time: The future in filters for cell phones," *IEEE Microw. Mag.*, vol. 16, no. 7, pp. 46–59, Aug. 2015.

[4] F. Balteanu, H. Modi, Y. Choi, J. Lee, S. Drogi, and S. Khesbak, "5G RF front end module architectures for mobile applications," in *Proc. 49th Eur. Microw. Conf. (EuMC)*, Paris, France, Oct. 2019, pp. 252–255.

[5] A. Giménez, J. Verdu, and P. De Paco Sánchez, "General synthesis methodology for the design of acoustic wave ladder filters and duplexers," *IEEE Access*, vol. 6, pp. 47969–47979, 2018.

[6] G. Ariturk, N. R. Almuqati, Y. Yu, E. T.-T. Yen, A. Fruehling, and H. H. Sigmarsson, "Exact synthesis of hybrid acoustic–electromagnetic filters with wideband Chebyshev responses," *IEEE Trans. Microw. Theory Techn.*, vol. 72, no. 5, pp. 3185–3199, May 2024.

[7] E. Guerrero, P. Silveira, J. Verdu, Y. Yang, S. Gong, and P. de Paco, "A synthesis approach to acoustic wave ladder filters and duplexers starting with shunt resonator," *IEEE Trans. Microw. Theory Techn.*, vol. 69, no. 1, pp. 629–638, Jan. 2021.

[8] S. Cano, C. Caballero, O. Barrera, R. Lu, J. Verdu, and P. de Paco, "General synthesis methodology for acoustic wave ladder filters in the bandpass domain," *IEEE Trans. Microw. Theory Techn.*, vol. 73, no. 10, pp. 7055–7068, Oct. 2025.

[9] S. Cano, J. Verdu, and P. de Paco, "Coupling matrix decomposition of acoustic wave ladder filters in the bandpass domain," *IEEE Trans. Microw. Theory Techn.*, vol. 74, no. 1, pp. 569–580, Jan. 2026.

[10] H. Tian, Y. Zheng, and Y. Dong, "Synthesis of ladder{-} and DMS-type acoustic wave filters and duplexers in bandpass domain," *IEEE Trans. Microw. Theory Techn.*, vol. 72, no. 8, pp. 4445–4456, Aug. 2024.

[11] R. J. Cameron, C. M. Kudsia, and R. R. Mansour, *Microwave Filters for Communication Systems*. Hoboken, NJ, USA: Wiley, 2018.

[12] S. Amari and G. Macchiarella, "Synthesis of inline filters with arbitrarily placed attenuation poles by using nonresonating nodes," *IEEE Trans. Microw. Theory Techn.*, vol. 53, no. 10, pp. 3075–3081, Oct. 2005.

[13] L. Acosta, E. Guerrero, P. Silveira, J. Verdu, and P. D. Paco, "Synthesis methodology of AW filters for RF applications based on matrix rotations to overcome round-off errors," in *Proc. IEEE Int. Ultrason. Symp. (IUS)*, Jun. 2021, pp. 1–4.

[14] R. M. Fano, "Theoretical limitations on the broadband matching of arbitrary impedances," *J. Franklin Inst.*, vol. 249, no. 1, pp. 57–83, Jan. 1950.

[15] J. Carlin and P. Civalleri, *Wideband Circuit Design*. Boca Raton, FL, USA: CRC Press, 1997.

[16] J. W. Helton, "Non-Euclidean functional analysis and electronics," *Bull. Amer. Math. Soc.*, vol. 7, no. 1, pp. 1–64, 1982.

[17] D. M. Martinez, "Méthodologies et outils de synthèse pour Des.fonctions de filtrage chargées par Des.impédances complexes," Ph.D. dissertation, Faculte des Sci. et Techn., L'universite de Limognes de Limognes, Limoges, France, 2019. [Online]. Available: http://www.theses.fr/2019LIMO0025/document

[18] G. Bose, F. Ferrero, L. Lizzi, D. Martinez, and F. Seyfert, "Convex optimization for the synthesis of matching filters," in *Proc. Int. Conf. Electromagn. Adv. Appl. (ICEAA)*, Sep. 2017, pp. 1450–1453.

[19] (2025). *Vector Fitting*. [Online]. Available: https://www.sintef.no/en/software/vector-fitting/downloads/#menu

[20] B. Gustavsen and A. Semlyen, "Rational approximation of frequency domain responses by vector fitting," *IEEE Trans. Power Del.*, vol. 14, no. 3, pp. 1052–1061, Jul. 1999.

[21] B. Gustavsen, "Improving the pole relocating properties of vector fitting," *IEEE Trans. Power Del.*, vol. 21, no. 3, pp. 1587–1592, Jul. 2006.

[22] D. Deschrijver, M. Mrozowski, T. Dhaene, and D. De Zutter, "Macromodeling of multiport systems using a fast implementation of the vector fitting method," *IEEE Microw. Wireless Compon. Lett.*, vol. 18, no. 6, pp. 383–385, Jun. 2008.

[23] C. Caballero, L. Acosta, E. Guerrero, J. Verdu, and P. De Paco, "Nonstandard transmission responses enabling feasible microwave-acoustic ladder filters," *IEEE Trans. Microw. Theory Techn.*, vol. 71, no. 9, pp. 3712–3721, Sep. 2023.

[24] S. Cano et al., "Enhanced modeling of wideband acoustic wave ladder filters," in *Proc. IEEE Int. Ultrason. Symp. (IUS)*, Jan. 2025, pp. 1–4.

[25] *Advanpix Multiprecision Computing Toolbox for MATLAB*. Accessed: Nov. 21, 2025. [Online]. Available: https://www.advanpix.com/

[26] S. Cano, M. Faura, J. Verdu, and P. De Paco, "Comparative study of durand–kerner and vector fitting as root-finding algorithms for the synthesis of high-order filters and multiplexers," in *Proc. IEEE Int. Microw. Filter Workshop (IMFW)*, Feb. 2026, pp. 1–3.

[27] S. Tamiazzo, G. Macchiarella, and F. Seyfert, "Path filters: A class of true inline topologies with transmission zeros," *IEEE Trans. Microw. Theory Techn.*, vol. 70, no. 1, pp. 850–863, Jan. 2022.

[28] A. Morini et al., "Systematic evaluation of spikes due to interference between cascaded filters," *IEEE Trans. Microw. Theory Techn.*, vol. 66, no. 11, pp. 4814–4819, Nov. 2018.

[29] L. Acosta, S. Cano, J. Verdu, and P. De Paco, "Avoidance of spurious spikes arisen by the cascading of filters through controlling filters input phases," in *Proc. IEEE Int. Ultrason. Symp. (IUS)*, Sep. 2023, pp. 1–4.

[30] *Menlo Microsystems Switch Mm5140*. Accessed: Oct. 28, 2025. [Online]. Available: https://menlomicro.com/resources/mm5140

[31] J. Anguera, A. Andujar, G. Mestre, J. Rahola, and J. Juntunen, "Design of multiband antenna systems for wireless devices using antenna boosters [Application notes]," *IEEE Microw. Mag.*, vol. 20, no. 12, pp. 102–114, Dec. 2019.

[32] N. T. J. Anguera and A. Andújar, *Slim radiating systems for electronic devices*, U.S. Patent 9 960 478 B2, May 1, 2018.

[33] K. Kurokawa, "Power waves and the scattering matrix," *IEEE Trans. Microw. Theory Techn.*, vol. MTT-13, no. 2, pp. 194–202, Mar. 1965.

[34] E. Guerrero, L. Acosta, J. Verdu, and P. de Paco, "Direct synthesis of acoustic wave multiplexers built on fully canonical multiport functions," *IEEE Trans. Microw. Theory Techn.*, vol. 71, no. 4, pp. 1391–1401, Apr. 2023.

Santi Cano (Graduate Student Member, IEEE) was born in Sabadell, Spain, in 2000. He received the B.S. and M.S. degrees in telecommunications engineering from the Universitat Autónoma de Barcelona (UAB), Barcelona, Spain, in 2021 and 2023, respectively, where he is currently pursuing the Ph.D. degree at the WavesLab Group.

His main research interests include the synthesis of microwave filters and the synthesis and design of microwave acoustic filters for wireless communications applications.

Mario Faura (Graduate Student Member, IEEE) was born in Barcelona, Spain, in 2000. He received the B.S. and M.S. degrees in telecommunications engineering from the Universitat Autónoma de Barcelona (UAB), Barcelona, in 2021 and 2023, respectively, where he is currently pursuing the Ph.D. degree at the WavesLab Group.

His main research interests include the synthesis of microwave filters and the synthesis and design of microwave acoustic filters and multiplexers.

Laia Garcia (Graduate Student Member, IEEE) was born in Granollers, Spain, in 2000. She received the B.S. and M.S. degrees in telecommunications engineering from the Universitat Autónoma de Barcelona (UAB), Barcelona, Spain, in 2021 and 2023, respectively, where she is currently pursuing the Ph.D. degree at the WavesLab Group.

Her main research interests include the identification of design deviations in microwave acoustic filters, as well as their synthesis and design for wireless communication applications.

Josep Parrón-Granados (Senior Member, IEEE) was born in Sabadell, Spain, in 1970. He received the M.S. degree in telecommunication engineering and the Ph.D. degree from the Universitat Politécnica de Catalunya (UPC), Barcelona, Spain, in 1994 and 2001, respectively.

From 2000 to 2002, he served as an Assistant Professor with the Electromagnetic and Photonic Engineering Group of the Signal Theory and Communication Department, UPC. In 2002, he joined as a Lecturer at the Telecommunication and Systems Engineering Department, Universitat Autónoma de Barcelona (UAB), Barcelona, where he was promoted to a Full Professor in 2024. He has co-authored 40 technical peer-reviewed journal articles and over 90 conference contributions. His current research interests include numerical methods for electromagnetism, antenna analysis and design, phased arrays, and reflective intelligent surfaces.

Pedro de Paco (Senior Member, IEEE) was born in Badalona, Spain. He received the M.S. degree in telecommunication engineering and the Ph.D. degree (cum laude) from the Universitat Politécnica de Catalunya (UPC), Barcelona, in 1997 and 2003, respectively.

In 1998, he joined the Electromagnetic and Photonics Engineering Group (EEF), Signal Theory and Communications Department (TSC), UPC, with a grant from the Institut d'Estudis Espacials de Catalunya (IEEC), Barcelona, in a joint activity related with European scientific space mission Planck. He was a member of the LFI-Radiometer Working Group and the Planck Consortium. During his Ph.D. at UPC stage, he has participated in several national and international research projects mostly related to microwave and millimeter-wave circuits and systems applied to the design and testing of remote sensing instruments and front-endpoint-to-multipoint broadband communication systems. Since 2004, he has been an Associate Professor with the Universitat Autónoma de Barcelona (UAB), Barcelona, where he teaches applied electromagnetics and microwave engineering courses. He has advised eight Ph.D. students. From 2010 to 2013, he was the Deputy Director and a member of the Executive Board at the Telecommunication and System Engineering Department, UAB. From 2018 to 2019, he was a Visiting Researcher with the Microwave and RF Research Group, University of Colorado at Boulder, Boulder, CO, USA. His main research interests include microwave filter synthesis and microwave acoustics filter synthesis and design, as well as microwave and radar systems and devices.

Dr. de Paco is a member of the MTT-6 RF MEMS and Microwave Acoustics Committee and a reviewer of IEEE TRANSACTIONS ON MICROWAVE THEORY AND TECHNIQUES and IEEE MICROWAVE AND WIRELESS COMPONENTS LETTERS. He serves as a member of the Technical Review Board for the European Microwave Conference. He has been appointed as a Technical Expert for Telecommunications Equipment by the National Agency of Accreditation. He was awarded three times with merits in research and recognized with merits in University training by l'Agéncia de Qualitat, and Advanced Research by Generalitat de Catalunya.